Structural basis for nonneutralizing antibody competition at antigenic site II of the respiratory syncytial virus fusion protein

Jarrod J. Mousa[a], Marion F. Sauer[b], Alexander M. Sevy[b], Jessica A. Finn[c], John T. Bates[a], Gabriela Alvarado[c], Hannah G. King[a], Leah B. Loerinc[a], Rachel H. Fong[d], Benjamin J. Doranz[d], Bruno E. Correia[e], Oleksandr Kalyuzhniy[e], Xiaolin Wen[f], Theodore S. Jardetzky[f], William R. Schief[e], Melanie D. Ohi[g], Jens Meiler[h], and James E. Crowe Jr.[a,c,i,1]

[a]Vanderbilt Vaccine Center, Vanderbilt University Medical Center, Nashville, TN 37232; [b]Chemical and Physical Biology Program, Vanderbilt University Medical Center, Nashville, TN 37232; [c]Department of Pathology, Microbiology, and Immunology, Vanderbilt University, Nashville, TN 37232; [d]Integral Molecular, Inc., Philadelphia, PA 19104; [e]Department of Immunology and Microbial Science, The Scripps Research Institute, La Jolla, CA 92037; [f]Department of Structural Biology, Stanford University School of Medicine, Stanford, CA 94305; [g]Department of Cell and Developmental Biology, Vanderbilt University Medical Center, Nashville, TN 37232; [h]Department of Chemistry, Vanderbilt University, Nashville, TN 37232; and [i]Department of Pediatrics, Vanderbilt University School of Medicine, Nashville, TN 37232

Edited by Rino Rappuoli, GSK Vaccines, Siena, Italy, and approved September 20, 2016 (received for review June 10, 2016)

Palivizumab was the first antiviral monoclonal antibody (mAb) approved for therapeutic use in humans, and remains a prophylactic treatment for infants at risk for severe disease because of respiratory syncytial virus (RSV). Palivizumab is an engineered humanized version of a murine mAb targeting antigenic site II of the RSV fusion (F) protein, a key target in vaccine development. There are limited reported naturally occurring human mAbs to site II; therefore, the structural basis for human antibody recognition of this major antigenic site is poorly understood. Here, we describe a nonneutralizing class of site II-specific mAbs that competed for binding with palivizumab to postfusion RSV F protein. We also describe two classes of site II-specific neutralizing mAbs, one of which escaped competition with nonneutralizing mAbs. An X-ray crystal structure of the neutralizing mAb 14N4 in complex with F protein showed that the binding angle at which human neutralizing mAbs interact with antigenic site II determines whether or not nonneutralizing antibodies compete with their binding. Fine-mapping studies determined that nonneutralizing mAbs that interfere with binding of neutralizing mAbs recognize site II with a pose that facilitates binding to an epitope containing F surface residues on a neighboring protomer. Neutralizing antibodies, like motavizumab and a new mAb designated 3J20 that escape interference by the inhibiting mAbs, avoid such contact by binding at an angle that is shifted away from the nonneutralizing site. Furthermore, binding to rationally and computationally designed site II helix–loop–helix epitope-scaffold vaccines distinguished neutralizing from nonneutralizing site II antibodies.

F protein | human respiratory syncytial virus | neutralizing antibodies

Respiratory syncytial virus (RSV) is a highly contagious human pathogen, infecting the majority of infants before age 2 y, and is the leading cause of viral bronchiolitis and viral pneumonia in infants and children (1, 2). RSV remains a top priority for vaccine development, as thousands of deaths are recorded worldwide each year because of complications from infection (3). To date, there is no licensed RSV vaccine. A major focus of RSV vaccine development has been inclusion of the RSV fusion (F) protein, a class I fusion glycoprotein that is synthesized as a precursor and cleaved into two disulfide-linked fragments upon maturation into a trimer (4). Although the RSV virion contains two additional surface proteins, the highly-glycosylated attachment (G) protein and the small hydrophobic protein, the F protein is highly conserved among strains of RSV strains and is the major target of protective neutralizing antibodies.

The F protein is known to adopt at least two major conformations: the metastable prefusion conformation and the postfusion conformation. Following attachment of the virion to a cell by the G protein, the F protein undergoes a dramatic structural rearrangement, resulting in fusion of the viral and cell membranes, and in cultured cells causes formation of cell syncytia. Four major neutralizing antigenic regions have been identified to date in the F protein, generally designated antigenic sites I, II, IV, and Ø, with the latter present only in the prefusion conformation. Site II is the target of palivizumab (5), a prophylactic treatment licensed for use in high-risk infants during the RSV season. An RSV F protein subunit vaccine candidate comprising aggregates of the postfusion conformation of RSV F is being tested currently in clinical trials (6), and serum antibody competition with palivizumab has been proposed as a potential serologic correlate of immunity for that vaccine (7, 8). We and others have isolated and studied RSV F-specific mAbs using murine hybridomas (9), sorted macaque B cells (10), and transformed human B cells or human antibody gene phage-display libraries (11, 12). Examples include mAbs 101F (9), D25 (13), and the next-generation site II mAb motavizumab (14). However, there are no reported naturally occurring human mAbs to site II, and palivizumab is an engineered

Significance

Respiratory syncytial virus is a highly contagious human pathogen, infecting the majority of infants before age 2 y, and is the leading cause of viral bronchiolitis and viral pneumonia in infants and children. An approved prophylactic humanized mouse monoclonal antibody, palivizumab, is currently the standard-of-care treatment for immunocompromised individuals, and competition with palivizumab has been proposed as the basis for measuring effective immune responses for vaccine trials. Using a combination of X-ray crystallography, hydrogen-deuterium exchange, and saturation alanine mutagenesis scanning, we show the structural basis for neutralization by a human antibody at the palivizumab antigenic site. Furthermore, we describe nonneutralizing antibodies that directly compete with palivizumab and another human antibody 14N4. Taken together, the data presented provide unique concepts in structure-based vaccine design.

Author contributions: J.J.M., B.J.D., T.S.J., W.R.S., M.D.O., J.M., and J.E.C. designed research; J.J.M., M.F.S., A.M.S., J.A.F., J.T.B., G.A., H.G.K., L.B.L., R.H.F., B.E.C., O.K., and X.W. performed research; J.J.M. and B.E.C. contributed new reagents/analytic tools; J.J.M., M.F.S., A.M.S., J.A.F., R.H.F., O.K., X.W., T.S.J., W.R.S., M.D.O., J.M., and J.E.C. analyzed data; and J.J.M. and J.E.C. wrote the paper.

Conflict of interest statement: W.R.S. is a founder of Compuvax, Inc. J.E.C. is a member of the Scientific Advisory Boards of Compuvax and Meissa Vaccines.

This article is a PNAS Direct Submission.

Data deposition: The atomic coordinates and structure factors have been deposited in the Protein Data Bank, www.pdb.org (PDB ID codes 5J3D and 5ITB).

[1]To whom correspondence should be addressed. Email: james.crowe@vanderbilt.edu.

This article contains supporting information online at www.pnas.org/lookup/suppl/doi:10.1073/pnas.1609449113/-/DCSupplemental.

humanized version of the murine mAb 1129 (15). Therefore, the repertoire of human antibodies interacting with site II and the structural basis for their recognition of this major antigenic site is poorly understood.

To characterize the human immune response to the RSV F protein, we isolated and characterized human mAbs targeting the RSV F protein, and in particular focused discovery efforts on antigenic site II. Defining the structural basis for interaction of site II-specific antibodies revealed new insights into the complexity of this site and diverse modes of recognition that determined whether or not site II competing human antibodies neutralize RSV.

Results

Antibody Isolation, Binding, and Neutralization. We isolated nine human mAbs from four human donors targeting the postfusion RSV F protein using human hybridoma technology (16). Transformed B cells generated from the B cells of adult human donors were screened by ELISA for reactivity to the RSV A2 F protein. Reactive cells were fused with myelomas to create hybridoma cell lines and plated in a 384-well plate. After 7 to 10 d, culture supernatants were screened for binding to recombinant, postfusion RSV A2 F protein. Cells from positive wells were expanded, respectively, into single wells in a 96-well culture plate using culture medium containing CpG, Chk2 inhibitor II, and irradiated heterologous human peripheral blood mononuclear cells (PBMCs). After 1 wk, culture supernatants were screened by ELISA for binding to recombinant, postfusion RSV A2 F protein. Clonal hybridomas were obtained by single-cell flow cytometric sorting, and isotyping analysis of purified mAbs showed them to be primarily of the IgG_1 subclass (Table 1). To assess whether the mAbs possessed neutralizing activity, purified mAbs were tested by a plaque reduction neutralization assay using RSV strain A2. As expected, serum from two donors neutralized RSV (Fig. S1). Of the mAbs isolated, 14N4, 13A8, and 3J20 neutralized virus, whereas the remaining mAbs failed to show neutralization activity when tested at concentrations up to 100 μg/mL. These three neutralizing mAbs had IC_{50} values less than 1 μg/mL (Table 1 and Fig. S1). Recombinantly expressed site II mAb motavizumab (14), and previously described mAbs to site IV (101F) (9) and site Ø (D25) (13), were also tested for comparison. Mab 13A8 possessed potency similar to that of motavizumab and D25. mAbs were tested for binding by ELISA to postfusion or prefusion-stabilized disulfide-cavity filling (DS-Cav1) or single chain-triple mutant (SC-TM) RSV strain A2 F proteins (17, 18) and postfusion F from RSV strain 18537 B (Table 1 and Fig. S2). Determination of EC_{50} values revealed that the three neutralizing mAbs bound to both prefusion and postfusion F proteins with equal affinity, agreeing with the conservation of the antigenic site II epitope between pre- and postfusion RSV F (Table 1 and Fig. S2). Furthermore, we did not detect major differences between binding to purified DS-Cav1 or SC-TM prefusion-stabilized F protein variants, suggesting the conformation of these antigens is similar at site II. Although the remaining mAbs did not neutralize RSV, EC_{50} values for binding in ELISA to postfusion F protein were similar for the neutralizing and nonneutralizing mAbs. These data suggest that the binding location or pose, rather than the affinity, is the critical determinant for RSV neutralization in this set of mAbs. mAbs 4E7, 4B6, 9J5, and 12I1 favored the postfusion conformation, based on differences in binding to stabilized prefusion versus postfusion F protein. Serum from two donors was also tested for binding, and no significant differences were observed among the two (Fig. S2).

Epitope Binning Reveals the Complexity of Site II. To determine putative binding sites for the isolated mAbs, real-time competition-binding studies were conducted with his-tagged RSV F proteins coupled to antipenta-his biosensor tips. We included recombinant forms of the previously described RSV mAbs 101F (site IV), 131-2a (site I) (19), palivizumab (site II), and motavizumab (site II) for comparative purposes in the competition-binding study on postfusion and prefusion F, because the epitopes for those mAbs have been defined previously. A complex array of five distinct competition-binding groups was observed for binding to postfusion F (Fig. 1*A*). The groups containing mAbs binding to antigenic sites I, II, and IV were identified using the control mAbs. Three mAbs targeted site I, a neutralizing epitope present near the membrane proximal region of the F protein. However, none of these mAbs possessed neutralizing activity. The previously reported murine mAb 131-2a exhibits a low level of neutralizing activity (13), but recognition of this epitope by human mAbs was not associated with neutralization, suggesting antigenic site I is not a major target of the human neutralizing antibody response. The remaining mAbs competed with antibodies directed to antigenic site II. Three mAbs (4B6, 9J5, 12I1) competed with site II-specific antibodies, yet failed to neutralize RSV, suggesting they do not bind in the correct orientation or they do not contact the full complement of critical amino acid residues in the site. The three neutralizing mAbs 14N4, 13A8, and 3J20 competed for binding to postfusion F with both palivizumab and motavizumab, as would be expected for mAbs targeting antigenic site II, yet subtle differences were observed among the

Table 1. Isotype, binding and neutralization features of nine new RSV F-specific human mAbs or control mAbs

				Neutralization (IC_{50}; ng/mL)	Binding to F protein for indicated strain (EC_{50}; ng/mL)			
Donor	Monoclonal antibody	IgG subclass	Light chain	RSV A2	RSV A2	RSV A2 DS-Cav1	RSV A2 SC-TM	RSV 18537 B
2	4E7	1	λ	>	19	>	110	21
2	10F13	1	κ	>	17	66	93	21
1	14C16	1	κ	>	19	110	95	20
3	4B6	3	λ	>	24	>	130	24
1	9J5	1	κ	>	30	>	150	40
1	12I1	1	λ	>	26	>	250	33
1	14N4	1	κ	695	78	70	57	57
4	13A8	1	κ	55	82	62	52	64
2	3J20	1	κ	377	84	60	48	50
Control mAbs	Motavizumab	1	κ	123	30	37	28	35
	101F	1	κ	402	50	62	80	45
	D25	1	κ	21	>	89	72	>

EC_{50} values correspond to the concentration at which half-maximum signal was obtained in ELISA, based on optical density at 405 nm. Neutralization values were determined using a plaque-reduction assay, where the IC_{50} corresponds to the mAb concentration at which 50% plaque reduction was observed. > indicates no signal was detected below 100 μg/mL in neutralization assays and 20 μg/mL in ELISA binding assays; DS-Cav1 and SC-TM represent prefusion stabilized RSV F.

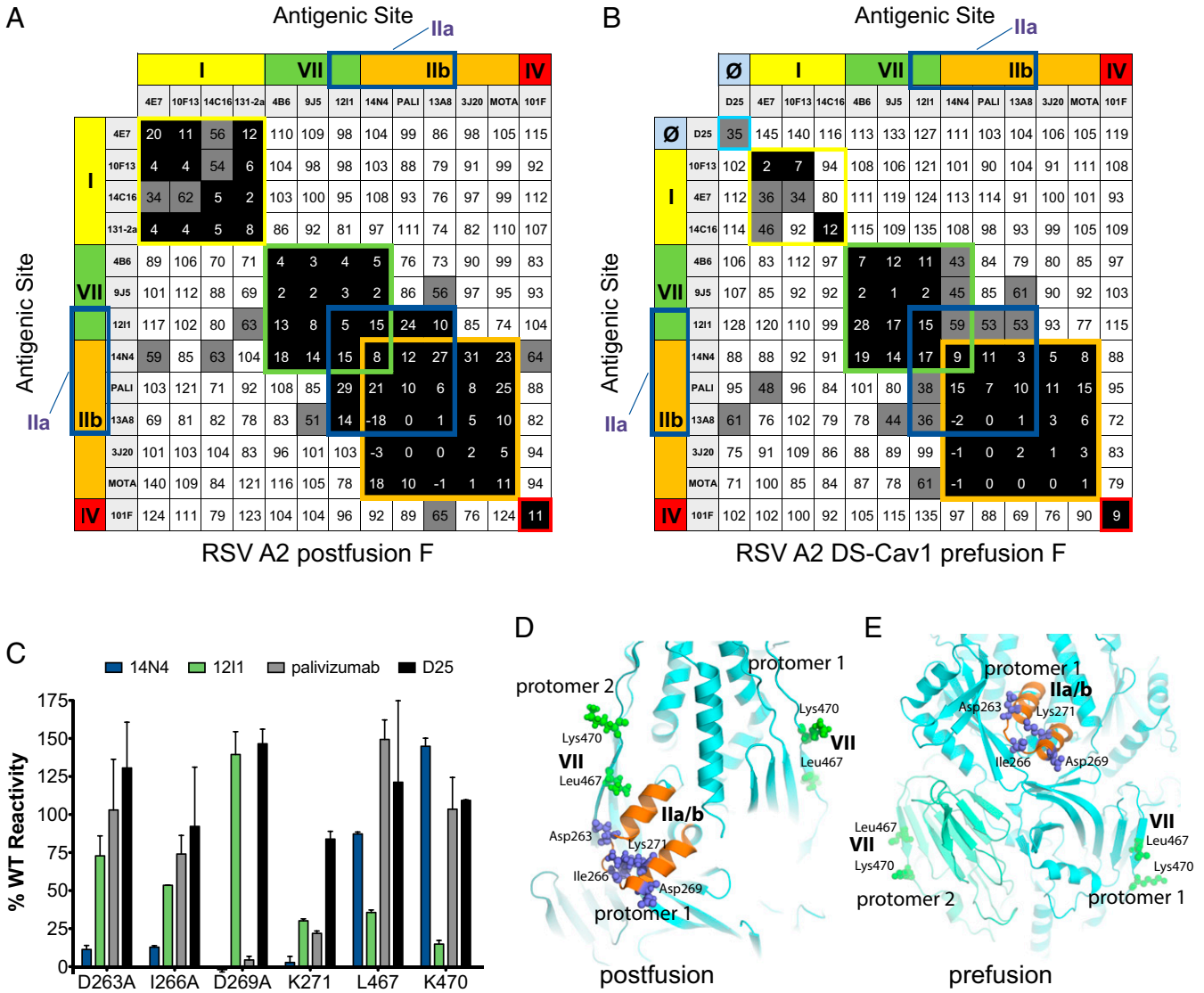

Fig. 1. Epitope binning and saturation alanine scanning mutagenesis for mAbs binding RSV F protein in the postfusion (*A*) or DS-Cav1 prefusion (*B*) conformations. Data indicate the percent binding of the competing antibody in the presence of the primary antibody, compared with the competing antibody alone. Cells filled in black indicate full competition, in which ≤33% of the uncompeted signal was observed, intermediate competition (gray) if signal was between 33% and 66%, and noncompeting (white) if signal was ≥66%. Antigenic sites are highlighted at the top and side based on competition-binding with the control mAbs D25 (site Ø), 131-2a (site I), palivizumab (PALI) or motavizumab (MOTA) (site II), or 101F (site IV). Competition for antigenic site II mAbs formed three groups, corresponding to site VII (green border), IIa (blue border), or IIb (orange border). Competition with nonneutralizing mAbs was less pronounced in the prefusion conformation. (*C*) Binding values for isolated mAbs 14N4 and 12I1 with palivizumab or D25 control mAbs. The mAb reactivity for each RSV F mutation was calculated relative to that of wild-type RSV F. Error bars indicate the measurement range. (*D*) The residues important for binding of 14N4 (blue) or 12I1 (green) are mapped on the RSV F trimeric structure as spheres. Residues important for 14N4 and 12I1 binding are very distant on the same protomer, yet are in close contact through quaternary interactions at the protomer 1–protomer 2 interface, leading to competition between neutralizing mAb 14N4 and nonneutralizing mAb 12I1. (*E*) Quaternary interactions between antigenic sites IIa and VII were less pronounced in the prefusion conformation, as site IIa is farther away from site VII on the same and adjacent protomers.

competition patterns. mAb 3J20 differed from the other two by competing only with other neutralizing mAbs. The most potent mAb, 13A8, showed ~50% competition with the nonneutralizing mAb 9J5 and directly competed with 12I1. Interestingly, mAb 14N4 directly competed with all three nonneutralizing mAbs, forming a block of four mAbs containing both neutralizing and nonneutralizing mAbs. Furthermore, intermediate one-directional competition was observed for 14N4 with site I mAbs 4E7 and 14C16.

Based on these data, it is apparent that mAbs competing for antigenic site II constitute at least three groups, which we designated antigenic sites IIa and IIb for neutralizing poses, and site VII for the nonneutralizing site. Antigenic site VII is represented by the nonneutralizing mAb 12I1. Antigenic site IIb, containing mAb 3J20 and motavizumab, is a discrete competition group containing only neutralizing mAbs. Antigenic site IIa is an intermediate site, distinguished from site IIb as competing with both neutralizing and nonneutralizing mAbs, and is recognized by mAbs 14N4, 13A8, and palivizumab. Further differences in competition patterns within the site IIa group of mAbs were observed, as 14N4 competes with all three nonneutralizing mAbs, 13A8 competes with two, and palivizumab competes with one, suggesting a gradient of binding poses occur at antigenic site IIa between sites VII and IIb. We also tested competition using prefusion F (DS-Cav1) as the immobilized antigen, and included the prefusion-specific mAb D25 for comparison (Fig. 1*B*). Although site VII

mAbs do not bind well to prefusion F protein by ELISA, we observed significant binding in biolayer interferometry experiments, allowing competition studies to be conducted with prefusion F. A similar pattern of three distinct groups was observed for antigenic site II in prefusion F; however, competition at site IIa was weaker among mAbs in the group, suggesting sites VII and IIa may be further apart in the prefusion than in the postfusion conformation. Such a complex array of competition-binding groups was unexpected, because the site II mAb palivizumab, which is used in prophylactic treatment, also bidirectionally competed with the nonneutralizing mAb 12I1. A palivizumab-competition assay designed to detect the presence of site II antibodies in immune serum by competing with palivizumab (7, 8) has been proposed as a correlate of immunity for an RSV postfusion F protein vaccine candidate. Indeed, we repeated the competition using published palivizumab competition assay protocols (7), where biotinylated palivizumab was spiked into control mAbs, as well as donor serum. As expected, we observed donor serum neutralized RSV and competed with palivizumab at low dilutions (Fig. S3). Furthermore, mAbs 14N4 and 12I1 both competed with palivizumab, with 12I1 showing competition only on postfusion F, similar to the competition data in Fig. 1.

Based on the data described, it appears motavizumab and 3J20-like mAbs may be better candidates for this purpose, as competition with these mAbs is observed only with neutralizing mAbs, but the palivizumab-competing antibody population contains a proportion of nonneutralizing mAbs. To determine if the nonneutralizing mAb 12I1 blocked neutralization of palivizumab or 14N4, we incubated mAb 12I1 with virus initially before applying the neutralizing mAbs. No significant difference was observed between those samples incubated with 12I1 and control mAbs (Fig. S3). This finding is expected as 12I1 favors the postfusion conformation (Table 1), which allows membrane fusion by the F protein before 12I1 binding. Thus, the site VII mAbs do not inhibit neutralization, yet are likely produced in response to a postfusion F immunogen, and also affect the palivizumab competition assay.

Saturation Alanine Scanning Mutagenesis. To better understand the complexity of antigenic site II and the specificity of mAbs recognizing the site, we performed saturation alanine scanning mutagenesis to identify residues critical for the binding of the neutralizing mAb 14N4 or nonneutralizing mAb 12I1. Residues Asp263, Ile266, Asp269, and Lys271 were critical for 14N4 binding (Fig. 1*C*). Interestingly, we previously identified a Ile266Met mutation when generating monoclonal antibody-resistant mutant (MARM) virus by in vitro selection using the RSV F targeting human Fab19 (11) isolated from a phage-display library. Based on the X-ray crystal structure of the RSV F protein (Fig. 1*D*), Ile266 is positioned at the bottom of the antigenic site II helix–loop–helix motif and is pointed toward the inner protein core, suggesting the residue disrupts the antigenic motif by allosteric effects. In the same study (11), selection with several murine mAbs produced MARM viruses with Lys272Asn, and similarly, selection with palivizumab in vitro or in vivo, generated similar MARM viruses with the following mutations: Lys272Met, Lys272Gln, and Asn268Ile (20, 21). The Lys272Gln MARM virus completely resisted prophylactic palivizumab treatment (22). Unexpectedly, mutagenesis scanning for the site VII mAb 12I1 revealed critical residues over 40 Å away in the RSV F monomer: Leu467 and Lys470 (Fig. 1 *C* and *D*). Although the site VII mAb 12I1 and site IIa mAb 14N4 competed for binding, the critical residues for binding were quite different, with site VII residues falling on the 47 Å extended loop connecting the lower structured portion to the helix bundle in a single protomer of F in postfusion conformation (Fig. 1*D*). However, when the F protein is viewed as a trimeric structure, all residues in antigenic sites VII and IIa come in close proximity through quaternary interactions. Antigenic site IIa in one protomer of F in the trimer is within 13 Å of antigenic site VII on an adjacent protomer. Although a quaternary epitope for RSV F has been described for the mAb AM14 (23), the site VII/IIa mAb competition is the first described example of quaternary interactions contributing to nonneutralizing mAb competition with a neutralizing mAb. In the prefusion conformation (Fig. 1*E*), antigenic sites VII and IIa are farther apart than in the postfusion form. Antigenic site IIa is equidistant from site VII on the same and the adjacent protomer. This difference confirms the observation in the epitope binning studies in which competition on prefusion F between antigenic sites IIa and VII was less pronounced than in the postfusion conformation. The intermediate level of competition for binding to the prefusion form of F between sites VII and IIa mAbs was consistent for mAbs 14N4, 13A8, and palivizumab.

Structure of the 14N4-Fab–RSV F Complex. Because 14N4 is a unique mAb, competing not only with palivizumab but also with nonneutralizing mAbs, we next sought to determine the structural basis for competition of 14N4 with other mAbs recognizing site II. The 14N4 fragment antigen-binding region (14N4-Fab) was crystallized in spacegroup $P\ 1\ 2_1\ 1$ and the structure was solved to 2.0 Å with R_{work}/R_{free} = 19.5/21.0% (Table S1). 14N4-Fab then was incubated with postfusion RSV A2 F, and the complex was isolated by size-exclusion chromatography and crystallized in spacegroup $P\ 4_2\ 2_1\ 2$. After screening with numerous cryoprotectants and attempts at data collection at room temperature, the best X-ray diffraction of the complex was to 4.1 Å (Table S1). The crystal structures of postfusion RSV F and 14N4 variable and constant Fab regions were used in molecular replacement to solve the structure of the complex with R_{work}/R_{free} = 25.6/28.2%, refined using noncrystallographic symmetry (NCS) torsion and reference-model restraints. Separate searches were needed for the variable and constant regions of the 14N4-Fab region as the constant region was shifted 56° from the apo–14N4-Fab structure, an observation likely attributed to crystal packing, as the constant region makes contacts to the next asymmetric unit (Fig. S4). The asymmetric unit is composed of the RSV F trimer with three 14N4-Fab molecules, one at each protomer of RSV F (Fig. 2*A*). Electron density for the RSV F protein and the three 14N4-Fab variable regions was well defined, especially at each interface between the two molecules (Fig. S5). To confirm binding at antigenic site II in RSV strain 18537 B, we complexed 14N4 with RSV 18537 B postfusion F and class-averages determined from negative-stain EM images indicated the position and orientation of the 14N4-Fab molecules were similar to those in the X-ray crystal structure (Fig. 2*A*). The heavy chain complementarity determining region 3 (HCDR3) of 14N4-Fab nestles between the two helices in the antigenic site II motif, where several hydrophobic residues exist. Residues in the RSV F structure important for binding based on alanine scanning mutagenesis are highlighted in Fig. 2*B*, where they make key interactions with 14N4-Fab. Asp263 is within hydrogen bonding distance of the backbone Gly56 on 14N4, and Lys271 likely interacts with the heavy-chain complementarity determining region (CDR)3 by hydrogen bonding with Thr107 (Fig. 2*B*). Furthermore, the light-chain also appears important for binding, because Asn99 and Ser37 of the light-chain CDR1 are in close contact with Asp269. Lys272 is near of the light-chain CDR2 Asp57, although this residue was not critical for binding in mutagenesis scanning experiments. As expected, interactions were not observed for Ile266, as this residue is buried at the base of the helix–loop–helix motif.

Compared with the structure of motavizumab in complex with the site II peptide, striking differences were observed. Overlaying at antigenic site II, the motavizumab angle of binding is significantly different, as it is shifted 42° from the 14N4 binding region in the direction away from the 12I1 site VII (Fig. 2*C*). This structural difference correlates with the lack of competition between antigenic site IIb mAbs motavizumab and 3J20, and the antigenic site VII nonneutralizing mAbs binding at Leu467 and Lys470. 14N4 could indeed block the binding of 12I1, because its binding pose is predicted to be shifted just 27° from site VII. However, motavizumab is shifted away from site IIa enough to prevent competition with mAb 12I1. Considering critical binding

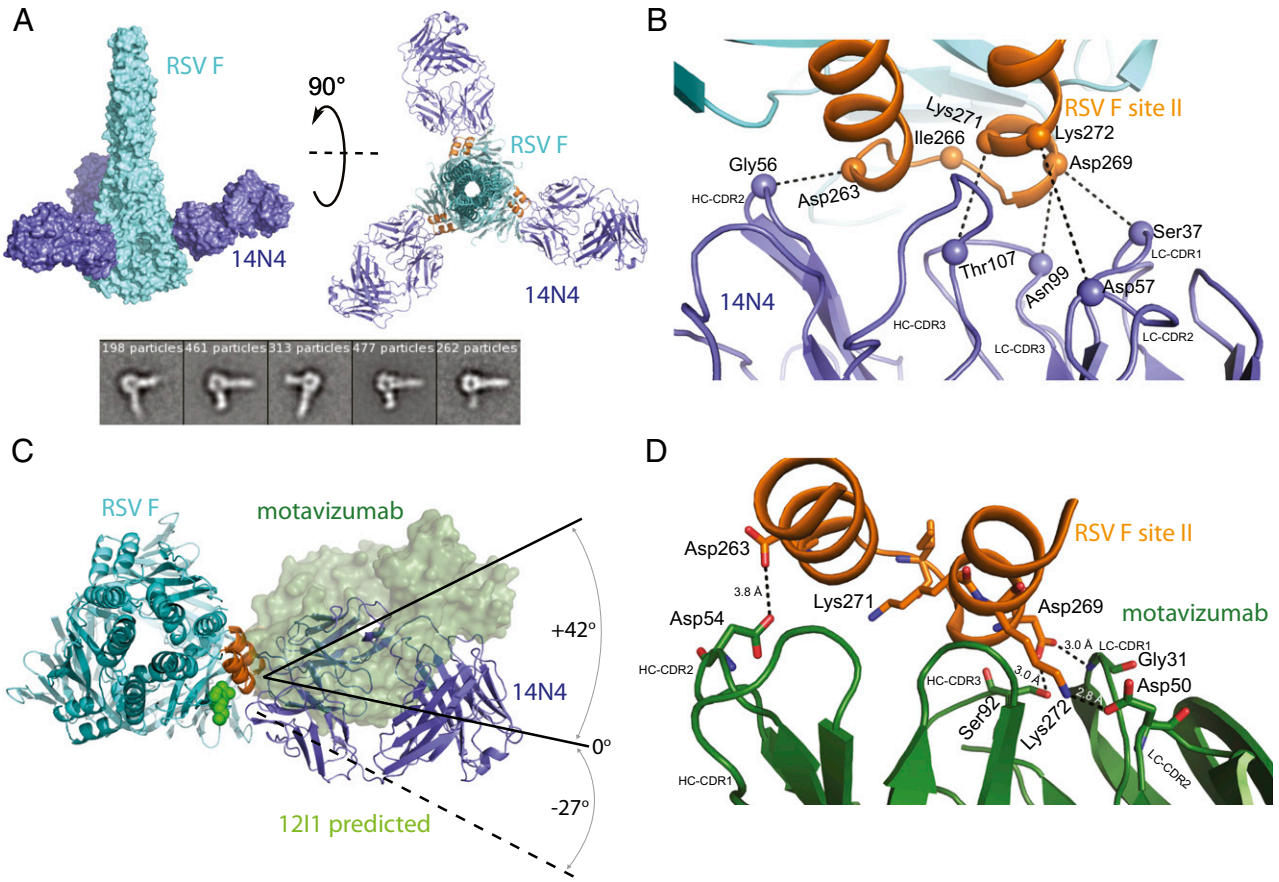

Fig. 2. The complex of 14N4-Fab with RSV F. (*A*) X-ray crystal structure of 14N4-Fab (blue) in complex with postfusion RSV strain A2 F protein (cyan). The overall structure is displayed in surface form and rotated 90° in cartoon form. 14N4-Fab bound RSV F at each protomer in the trimeric structure. EM class averages with RSV 18537 B are also displayed, confirming the binding location of 14N4-Fab. The side length of panels is 32.7 nm. (*B*) Chemical interactions between Fab 14N4 and RSV strain A2 F protein. Several key hydrogen bonds are important for molecular recognition. (*C*) Overlay of the complex with the motavizumab–site II peptide complex (PDB ID code 3IXT). Motavizumab is shown in green surface form, RSV F in cyan, and 14N4-Fab in blue. The antigenic site II region is colored in orange, and residues important for site VII binding are shown as spheres in light green. Motavizumab binds antigenic site II at a different orientation than 14N4-Fab, allowing it to be free of interactions with site VII. (*D*) Interactions between motavizumab and the antigenic site II peptide (PDB ID code 3IXT). Lys271 does not interact with motavizumab, unlike its role in the 14N4–RSV F complex.

interactions, we noted that motavizumab hydrogen bonds to Asp263 using Asp54 (HCDR2) distantly, to Lys272 with Asp50 [light chain complementarity determining region (LCDR2)], and Asp269 using Ser92 (LCDR3) (Fig. 2*D*). Interestingly, motavizumab bypasses Lys271, leaving no residues in the vicinity with which to interact. This positioning causes a shift away from site VII, as the majority of the interactions are involved on the right helix, rather than the left helix, where only hydrophobic interactions exist with the motavizumab HCDR3.

Human Antibodies Bind Scaffold-Based Immunogens. Attempts to generate a vaccine against RSV have been largely unsuccessful, and the presence of nonneutralizing mAbs competing with neutralizing mAbs may contribute to this problem. We and others have recently reported structure-based designed vaccine candidates for presenting the site II immunogen. Strategies included a stable trihelix scaffold protein purpose-built to support the helix–loop–helix motif of antigenic site II (FFL_001) (10), a Fab-based scaffold for site II (24), and also a strategy in which the RSV F site II was grafted onto the metapneumovirus (MPV) F protein (RPM-1) to generate a chimeric protein capable of inducing a cross-reactive immunogenic response (25) (Fig. 3*A*). Each of these three epitope-based scaffolds induced at least partial immune responses in mice to RSV F, and the FFL_001 vaccine candidate induced reasonable titers of neutralizing mAbs from immunized macaques. We tested binding by ELISA of the three neutralizing site II human mAbs 14N4, 13A8, and 3J20 to FFL_001 and RPM-1 and found that they did bind, as did palivizumab and motavizumab used as positive controls (Fig. 3*B*). EC_{50} values for binding of the mAbs to the scaffolded epitopes were similar to those obtained for the RSV F protein, suggesting antigenic site II is the primary region necessary for human mAb binding. This finding also is consistent with the X-ray crystallography and EM structural data for the 14N4-Fab–RSV F complex. Interestingly, binding was not detected for the nonneutralizing mAb 12I1 or other antigenic site VII mAbs to either FFL_001 or RPM-1 scaffold proteins. Therefore, binding to the scaffolded epitopes distinguishes neutralizing from nonneutralizing site VII competing antibodies. Surface plasmon resonance revealed very low K_D values for the three neutralizing mAbs (Fig. 3*C*), suggesting limited residues are needed for Fab binding to antigenic site II, a finding consistent with the X-ray structure of 14N4-Fab with RSV F, as no molecular contacts were observed outside site II. However, additional interacting residues may be present in 14N4 binding to prefusion RSV F. Binding was not detected to a mutated FFL_001 control (Fig. S6).

To confirm the binding location for 14N4 to the FFL_001 scaffolded epitope, we performed hydrogen-deuterium (HD) exchange mass spectrometry (Fig. 4*A*). We mapped the majority of the 14N4-Fab region (Fig. S7), and the peptides with the largest decrease in deuterium exchange in the bound state were localized to the HCDR3 loop, with a limited effect in the LCDR2. This finding is

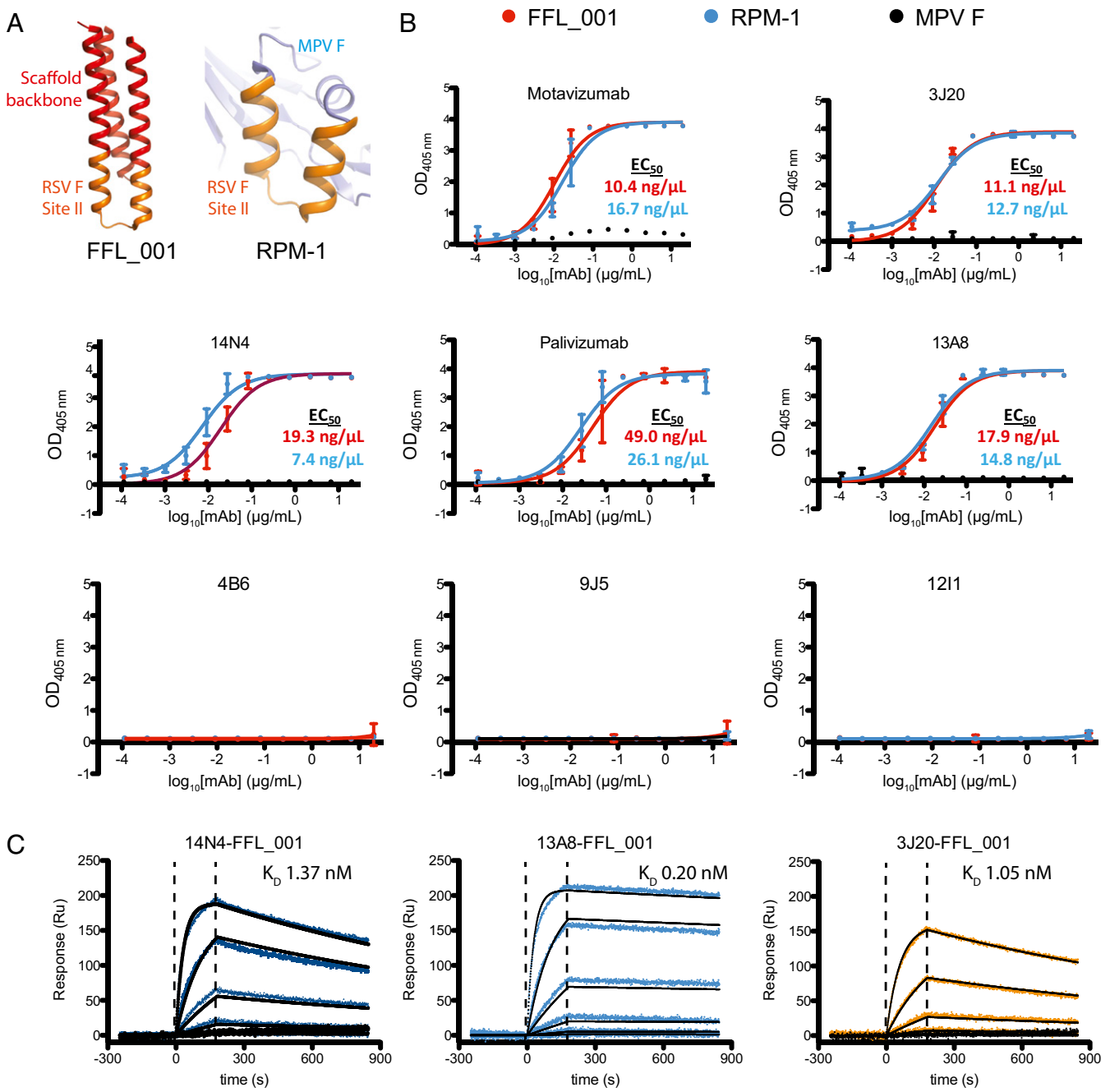

Fig. 3. Human mAbs bind to synthetic immunogens. (*A*) X-ray structure of FFL_001 displayed in red with RSV antigenic site VII shown in orange (PDB ID code 4JLR). A model of RPM-1 shows the region surrounding the corresponding antigenic site VII in the MPV F protein (blue, PDB ID code 4DAG), and RSV antigenic site II is overlaid in orange. (*B*) ELISA binding curves for three human mAbs 14N4, 13A8, and 3J20 along with antigenic site VII mAbs motavizumab and palivizumab. Binding curves for FFL_001 are in red and for RPM-1 are in blue. Binding to MPV F protein is shown in black. EC_{50} values are displayed for each, in corresponding colors. Error bars indicate 95% confidence intervals. (*C*) Surface plasmon resonance of 14N4, 13A8, and 3J20 Fabs binding to FFL_001 with calculated K_D values displayed. Colored data points are overlaid with the curve fit line in black. Dotted lines indicate the start of association and dissociation steps.

largely consistent with the crystal structure of 14N4-Fab with RSV F, as the HCDR3 is buried in the antigenic site II motif and the LCDR2 makes interactions through Asp57. These data suggest that 14N4 binds the scaffolded epitope using similar residues as with RSV F. Indeed, significant differences were not observed between X-ray structures of motavizumab in complex with FFL_001 and motavizumab in complex with the antigenic site II peptide (10), further suggesting the scaffold-based approach allows similar binding poses. We also compared the binding poses of the neutralizing macaque mAb 17HD9, isolated following FFL_001 immunization, and crystallized in complex with FFL_001 (10). mAb 17HD9 has an extended HCDR3 compared with 14N4 and motavizumab, and is positioned horizontally across the antigenic site II motif, unlike 14N4, where the HCDR3 is positioned vertically, inserting itself between the two helices (Fig. 4*B*). The extended CDR3 residues Arg109 and Asp107 make contacts with Lys271 and Lys272. Furthermore, the LC-CDR loops are positioned to make key contacts with the bottom of helix 2, a feature that allows mAb 17HD9 to interact with antigenic site II at a different angle, where the Fab is shifted downward

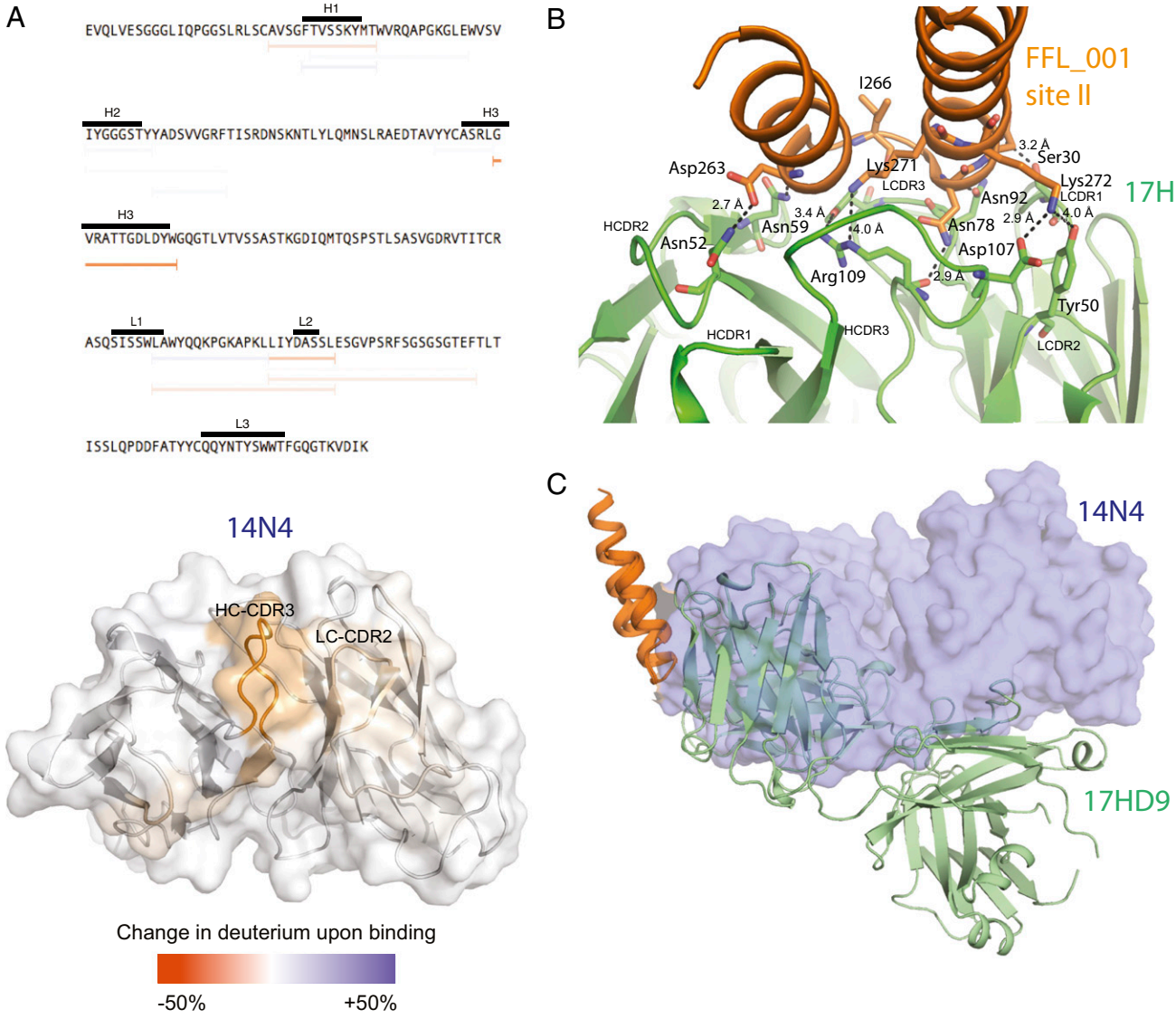

Fig. 4. HD exchange with FFL_001 and comparison with mab 17HD9. (*A*) HD exchange protection of 14N4 upon scaffold binding. Each antibody-derived peptide was monitored for deuterium incorporation in the presence or absence of the scaffold protein. Peptides are colored according to the difference in incorporated deuterium atoms in the bound vs. unbound form, with a large reduction in incorporation indicating a putative binding site (orange). Values from the 30-min deuteration time point are shown. The HD exchange profile of 14N4-derived peptides is mapped onto the 14N4 Fab structure. (*B*) Interactions between the macaque Fab 17HD9 and FFL_001 (PDB ID code 4N9G). (*C*) Overlay of 14N4 with antigenic site II and 17HD9 with FFL_001. 14N4 is displayed as surface form in blue, and 17HD9 in pale-green (PDB ID code 4N9G). 17HD9 interacts with the lower loop of antigenic site II along with both helices, whereas 14N4 interacts only with the two helices.

compared with 14N4 and motavizumab (Fig. 4*C*). mAb 17HD9 is positioned further left than 14N4, close to antigenic site VII, suggesting that 17HD9 would compete with 12I1 and other site VII mAbs. Indeed, we observed such competition between recombinantly expressed mAb 17HD9 and site VII mAbs (Fig. S8).

mAb 14N4 uses V_H3-53 and J_H4 gene segments to encode the expressed antibody (HCDR3 numbering in Fig. S9). Because of the paucity of human antibodies that target RSV antigenic site II, it was unclear if this mAb is unique among human donors, or if 14N4-like mAbs exist that do compete with nonneutralizing mAbs in the general population. To help answer this question, we searched a database of 50 million antibody heavy-chain variable sequences obtained from 31 adult human subjects, and found similar sequences in 31 individuals that used V_H3-53 and J_H4 gene segments and shared 85% similarity in the HCDR3 (Table 2). When the HCDR3 identity cut-off for matching was extended to 100%, the majority of sequence matches remained. These sequence homology data suggest that 14N4-like mAbs may be common in the human population, and the presence of nonneutralizing mAbs competing with neutralizing mAbs may be a common feature in human RSV immune responses.

Discussion

Although palivizumab has been used as a prophylactic treatment for high-risk infants during RSV season for nearly two decades, no vaccine is currently approved for protection against RSV. Vaccine strategies have been proposed that focus on the 150-kDa postfusion RSV F trimeric protein to elicit an immune response, yet antibody production is directed toward both protective and nonprotective epitopes. We have shown in the described human mAbs evidence for substantial neutralizing/nonneutralizing mAb competition binding at antigenic site II. Considering the competition patterns, antigenic site II was delineated into two subsites based on epitopes on adjacent protomers of the RSV F

trimer, and a new region, site VII, was characterized as a nonneutralizing antigenic site that competes with site II. Based on the X-ray structure of 14N4 in complex with RSV F, subtle changes in the binding pose can cause substantial effects in competing antibodies. Although the competition was described here for RSV, these data may inform general vaccine design, as nonneutralizing antibody production is a common occurrence during viral infection. Furthermore, studying the B-cell response of vaccinated individuals in clinical trials will assist in determining the extent of neutralizing/nonneutralizing mAb competition in human sera.

Competition between 14N4 and 12I1 mAbs on postfusion F is readily observed, as the 12I1 site VII is in close proximity to antigenic site IIa. However, the competition was less pronounced in the prefusion conformation, as sites VII and IIa are not in close proximity before the pre- to postfusion rearrangement. Because 12I1 favors the postfusion conformation (Table 1), vaccine strategies involving prefusion F may be more beneficial to avoiding the competing interactions at antigenic site II. Indeed, 12I1 was likely generated against the RSV F postfusion conformation, and these 12I1-like mAbs may not have been isolated if prefusion F was used in the initial B-cell isolation. Future experiments detailing the mAb response to prefusion F will be beneficial in determining the overall impact of the competition with nonneutralizing mAbs. When assessing vaccine efficacy using competition with palivizumab, nonneutralizing antibody competition with palivizumab must be taken into account, especially in vaccine candidates using postfusion RSV F. We further propose using motavizumab or other 3J20-like mAbs rather than palivizumab in serum antibody competition-binding assays to monitor neutralizing mAbs, as motavizumab competes only with neutralizing mAbs.

As an alternative to full-length RSV F as a vaccine strategy, our data support the concept of using scaffold-based epitopes for immunization against RSV. For example, FFL_001 avoids the potential for nonneutralizing 12I1-like mAb production to compete for binding with neutralizing 14N4-like mAbs, because only the neutralizing epitope is present for an immune response, unlike RSV F, where the 12I1 site VII is on an adjacent protomer. Binding to RPM-1 also provides insight into the neutralizing site II epitope, because homologous residues exist in the MPV protein near site VII, yet nonneutralizing RSV-specific antibodies do not bind RPM-1. Thus, these scaffold-based immunogens can be used to identify neutralizing mAbs targeting site II, instead of intact RSV F, which also binds nonneutralizing antibodies. As potential vaccines, epitope-scaffold immunogens would not induce site VII mAbs, likely producing only neutralizing mAbs to antigenic site II.

In summary, careful study of the fine specificity of new human antibodies to the RSV F antigenic site II revealed important structural features that inform next-generation vaccine design and testing, and provide potently neutralizing candidate prophylactic human mAbs.

Table 2. Identification of mAb 14N4-like sequences in a healthy human donor antibody heavy-chain variable gene sequence database

	Number of variable region sequences identified at indicated percentage match in the HCDR3	
Donor	85%	100%
A	118	99
B	39	33
C	37	36
D	458	398
E	437	387
F	1	1
G	1	1
H	5	5
I	81	68
J	3	3
K	1	1
L	3	3
M	1	1
N	2	2

Sequences related to 14N4 are found in many donors. From our database of 50M+ sequences, we identified unique functional sequences (i.e., sequences without stop codons) related to 14N4 using the following clustering protocol: to be considered related, sequences must use the same V and J gene as 14N4 (here, IGHV3-53/IGHJ4) and their HCDR3 amino acid sequence must group with 14N4 when clustered at 85% identity using CD-HIT. Of the related sequences, many of them used the 14N4 HCDR3 with no amino acid mutations (100% match).

Materials and Methods

ELISA for Binding to RSV F Protein. For recombinant protein capture ELISA, 384-well plates were treated with 2 μg/mL of antigen for 1 h at 37 °C or overnight at 4 °C. Following this procedure, plates were blocked for 1 h with 2% (wt/vol) milk supplemented with 2% (vol/vol) goat serum. Primary mAbs and culture supernatants were applied to wells for 1 h following three washes with PBS-T. Plates were washed with PBS-T four times before applying 25 μL secondary antibody (goat anti-human IgG Fc; Meridian Life Science) at a dilution of 1:4,000 in blocking solution. After 1 h incubation, the plates were washed five times with PBS-T, and 25 μL of phosphatase substrate solution (1 mg/mL phosphatase substrate in 1 M Tris aminomethane; Sigma) was added to each well. The plates were incubated at room temperature before reading the optical density at 405 nm on a Biotek plate reader. The palivizumab competition assay ELISA was conducted by coating ELISA plates with the desired 2 μg/mL of the desired antigen. Next, serially diluted competing mAbs spiked with 50 ng/mL biotinylated palivizumab were added to the plates. Alternatively, serially diluted serum was spiked with 50 ng/mL biotinylated palivizumab. Control wells contained PBS with 50 ng/mL biotinylated palivizumab. Palivizumab was biotinylated using the EZ-Link NHS PEG4 Biotinylation Kit (ThermoFisher) following the manufacturer's protocol. After 1-h incubation, the plates were washed with PBS-T and streptavidin-HRP (ThermoFisher) diluted 1:4,000 in blocking solution was applied for 1 h. After a washing step, plates were incubated with one-step Ultra TMB solution (ThermoFisher). The reaction was stopped by adding an equal volume of 1 M HCl. Plates were read on a Biotek plate reader at 450 nm.

Human Hybridoma Generation. Participation of healthy human adult subjects was approved by the Vanderbilt University Institutional Review Board, and blood samples were obtained only after informed consent. PBMCs were isolated from human donor blood samples using Ficoll-Histopaque density gradient centrifugation. Approximately 10 million PBMCs were mixed with 17 mL of ClonaCell-HY Medium A (StemCell Technologies), 8 μg/mL of CpG (phosphorothioate-modified oligodeoxynucleotide ZOEZOEZZZZZOEEZOEZZZT; Invitrogen), 3 μg/mL of Chk2 inhibitor II (Sigma), 1 μg/mL of cyclosporine A (Sigma), and 4.5 mL of filtered supernatant from a culture of B95.8 cells (ATCC VR-1492) containing Epstein-Barr virus and plated in a 384-well plate. After 7 to 10 d, culture supernatants were screened for binding to recombinant, postfusion RSV strain A2 F protein and FFL_001. Cells from positive wells were expanded into single wells in a 96-well culture plate using culture medium containing 8 μg/mL CpG, 3 μg/mL Chk2 inhibitor II, and irritated heterologous human PBMCs (Nashville Red Cross). After 1 wk, culture supernatants were screened by ELISA for binding to recombinant, postfusion RSV A2 F protein and FFL_001. Cells from positive wells were fused with HMMA2.5 myeloma cells by electrofusion (26). Fused cells were plated in 384-well plates in growth medium containing 100 μM hypoxanthine, 0.4 μM aminopterin, 16 μM thymidine (HAT Media Supplement, Sigma), and 7 μg/mL ouabain (Sigma). Hybridomas were screened after 2 wk for mAb production by ELISA, and cells from wells with reactive supernatants were expanded to 48-well plates for 1 wk before being screened again by ELISA, and then subjected to single-cell fluorescence-activated sorting. After cell sorting into 384-well plates containing Medium E (StemCell Technologies), hybridomas were screened by ELISA before expansion into both 48-well and 12-well plates.

Human mAb and Fab Production and Purification. Hybridoma cells lines were expanded in Medium E until 80% confluent in 75-cm^2 flasks. For antibody production, cells from one 75-cm^2 cell culture flask were collected with a cell scraper and expanded to four 225-cm^2 cell culture flasks in serum-free medium (Hybridoma-SFM, Gibco). After 21 d, supernatants were sterile filtered

using 0.45-μm pore size filter devices. For antibody purification, HiTrap MabSelectSure columns (GE Healthcare Life Sciences) were used to purify antibodies using the manufacturer's protocol. To obtain Fab fragments, papain digestion was used (Pierce Fab Preparation Kit, Thermo Scientific). Fab fragments were purified by removing IgG and Fc contaminants using a HiTrap MabSelectSure followed by purification with an anti-CH1 column (GE Healthcare Life Sciences).

Production and Purification of Recombinant RSV F Protein RSV mAbs, and Epitope Immunogens. Plasmids encoding cDNAs for RSV subgroup A strain A2 or subgroup B strain 18537 prefusion (DS-Cav1) and postfusion F protein constructs (a gift from Barney Graham, Viral Pathogenesis Laboratory, National Institutes of Health, Bethesda) were expanded in *Escherichia coli* DH5α cells and plasmids were purified using Qiagen Plasmid Maxiprep kits (Qiagen). Prefusion-stabilized RSV F SC-TM was synthesized (Genscript). Plasmids encoding cDNAs for the the protein sequences of mAb 101F and mAb D25 were synthesized (Genscript), and heavy- and light-chain sequences were cloned into vectors encoding human IgG1 and λ or κ light-chain constant regions, respectively. Mab 131-2a protein was obtained from Sigma. Commercial preparations of palivizumab (Medimmune) were obtained from the pharmacy at Vanderbilt University Medical Center. For each liter of protein expression, 1.3 mg of plasmid DNA was mixed with 2 mg of polyethylenimine in Opti-MEM I + GlutaMAX cell culture medium (Fisher). After 10 min, the DNA mixture was added to HEK293 cells at 1×10^6 cells per milliliter. The culture supernatant was harvested after 6 d, and the protein was purified by HiTrap Talon crude (GE Healthcare Life Sciences) column for RSV F protein variants or HiTrap MabSelectSure columns for mAbs, following the manufacturer's protocol. 14N4-Fab heavy and light variable region DNA was synthesized (Genscript) and cloned into vectors containing human CH1 and kappa sequences. 14N4-Fab was expressed in Expi293 (Invitrogen) cells using Expifectamine 293 (Invitrogen) following the manufacturer's protocol. Recombinant Fab was purified using anti-CH1 Capture Select column (GE Healthcare Life Sciences). FFL_001, FFL_001 mutant proteins, and RPM-1 were expressed and purified as described previously (10, 25). mAb 17HD9 was expressed in expi293F cells following the manufacturer's protocol, and using the vectors described previously (10).

RSV Plaque Neutralization Experiments. mAbs isolated from hybridoma supernatants were incubated 1:1 with a suspension of infectious RSV strain A2 for 1 h. Following this process, confluent HEp-2 cells, maintained in Opti-MEM I+GlutaMAX (Fisher) supplemented with 2% (vol/vol) FBS at 37 °C in a CO_2 incubator, in 24-well plates, were inoculated with 50 μL of the antibody:virus or serum:virus mixture for 1 h. After the hour, cells were overlaid with 1 mL of 0.75% methylcellulose dissolved in Opti-MEM I + GlutaMAX. Cells were incubated for 4 d after which the plaques were visualized by fixing cells with 10% (vol/vol) neutral-buffered formalin and staining with Crystal violet. Plaques were counted and compared with a virus control. Data were analyzed with Prism software (GraphPad) to obtain IC_{50} values. To determine competition with 12I1, virus was first mixed with 40 μg/mL 12I1 for 1 h. The virus:12I1 mixture was overlaid onto serial dilutions of 14N4 and palivizumab for 1 h. The rest of the process was completed as described above.

Assays for Competition-Binding. After obtaining an initial baseline in kinetics buffer (ForteBio; diluted 1:10 in PBS), 10 μg/mL of his-tagged RSV F protein was immobilized onto antipenta-his biosensor tips for a biolayer interferometry instrument (Octet Red, ForteBio) for 120 s. The baseline signal was measured again for 60 s before biosensor tips were immersed into wells containing 100 μg/mL primary antibody for 300 s. Following this process, biosensors were immersed into wells containing 100 μg/mL of a second mAb for 300 s. Percent binding of a second mAbs in the presence of the first mAb was determined by comparing the maximal signal of the second mAb after the first mAb was added to the maximum signal of the second mAb alone. mAbs were considered noncompeting if maximum binding of the second mAb was ≥66% of its uncompeted binding. A level between 33% and 66% of its uncompeted binding was considered intermediate competition, and ≤33% was considered competing.

Antibody Epitope Mapping. Shotgun mutagenesis epitope mapping of anti–RSV-F antibodies was performed using an alanine scanning mutagenesis library for RSV F protein (hRSV-A2; NCBI ref # FJ614814), covering 368 surface-exposed residues identified from crystal structures of both the prefusion and postfusion conformations of RSV F. An RSV F expression construct was mutated to change each residue to an alanine (and alanine residues to serine). The resulting 368 mutant RSV F expression constructs were sequence confirmed and arrayed into a 384-well plate (one mutation per well).

Library screening was performed essentially as described previously (27). The RSV F alanine scan library clones were transfected individually into human HEK-293T cells and allowed to express for 16 h before fixing cells in 4% (vol/vol) paraformaldehyde (Electron Microscopy Sciences) in PBS plus calcium and magnesium. Cells were incubated with mAbs, diluted in 10% (vol/vol) normal goat serum (NGS), for 1 h at room temperature, followed by a 30 min incubation with 3.75 μg/mL Alexa Fluor 488-conjugated secondary antibody (Jackson ImmunoResearch Laboratories) in 10% NGS. Cells were washed twice with PBS without calcium or magnesium and resuspended in Cellstripper (Cellgro) plus 0.1% BSA (Sigma-Aldrich). Cellular fluorescence was detected using the Intellicyt high-throughput flow cytometer (Intellicyt). Before library screening, to ensure that the signals were within the linear range of detection, the optimal screening concentrations for each mAb were determined using an independent immunofluorescence titration curve against cells expressing wild-type RSV F.

Antibody reactivity against each mutant protein clone was calculated relative to wild-type protein reactivity by subtracting the signal from mock-transfected controls and normalizing to the signal from wild-type protein-transfected controls. Mutations within clones were identified as critical to the mAb epitope if they did not support reactivity of the test mAb, but supported reactivity of other antibodies. This counter-screen strategy facilitates the exclusion of RSV F protein mutants that are misfolded or have an expression defect. The detailed algorithms used to interpret shotgun mutagenesis data are described elsewhere (27).

Crystallization and Structure Determination of 14N4-Fab and 14N4-Fab–RSV F. Recombinant 14N4-Fab was concentrated to 10 mg/mL and a crystal was obtained in Hampton Index HT screen condition 20% (wt/vol) PEG 3350, 50 mM zinc acetate. The crystal was harvested directly from the screening tray, cryoprotected in the mother liquor with 20% (vol/vol) glycerol, and data were collected using a Bruker Microstar microfocus rotating-anode X-ray generator equipped with a Bruker Proteum PT135 CCD area detector, and Proteium2 software (Bruker-AXS). Data were processed with XPREP (28) to 2.0 Å. The structure of 14N4-Fab were determined by molecular replacement in Phaser (29) using the separate constant and variable domain models from PDB ID code 4Q9Q. The model was improved through iterative refinements in Phenix (29) and manual building in Coot (30), guided by composite omit maps.

To crystallize 14N4 in complex with RSV F, both hybridoma-cleaved 14N4 and RSV A2 F were buffer-exchanged in excess into 50 mM Tris pH 7.5, 50 mM NaCl. 14N4-Fab was mixed in excess with RSV A2 F postfusion protein and incubated at 37 °C for 2 h. Following this, the sample was subjected to size-exclusion chromatography (S200, 16/300; GE Healthcare Life Sciences) in 50 mM Tris pH 7.5, 50 mM NaCl. The complex was concentrated to 10 mg/mL and crystals were obtained in Hampton Crystal Screen HT in 2 M ammonium sulfate, 5% (vol/vol) 2-propanol. Approximately 40 crystals were screened for diffraction, and numerous cryoprotectants were tried; however, the best diffraction obtained was to 4.1 Å using the mother liquor with 20% (vol/vol) glycerol as a cryoprotectant. X-ray diffraction data were collected at the Advanced Photon Source LS-CAT beamline 21-ID-F. Data were indexed and scaled using XDS (31). A molecular replacement solution was obtained in Phaser (29) using RSV A2 F protein trimer PDB ID code 3RRR and the structure of 14N4-Fv region. Significant density, albeit shifted from the apo-structure, was observed for the constant region, and a solution could be obtained in Phaser with the constant region. The structure was refined using group B-factors, coordinates, NCS restraints, and 14N4-Fab and PDB ID code 3RRR as reference models restraints. The density around the 14N4–RSV F interface was well defined and CDR loops matched well with the apo–14N4 structure. Data collection and refinement statistics are shown in Table S1.

Negative-Stain Electron Microscopy. 14N4-Fab was mixed in excess with RSV 18537 B postfusion F protein and incubated at 37 °C for 1 h. Following this, the complex was purified by size-exclusion chromatography (S200, 16/300; GE Healthcare Life Sciences) in 50 mM Tris pH 7.5, 50 mM NaCl. Carbon-coated copper grids were overlaid with the complex at 5 μg/mL for 3 min. The sample was washed in water twice and then stained with 0.75% uranyl formate for 1 min. Negative-stain micrographs were acquired using an FEI Tecnai F-20 transmission EM scope and a Gatan 4k × 4k CCD camera using 50,000× magnification at a defocus of −1.5 μm. Micrographs were rescaled by a factor of two resulting in a final image with 4.36Å/px. Particles were picked manually using EMAN Boxer (32) with a box size of 75 pixels and pixel size of 5.25 nm/px. Reference-free 2D classification was performed using Spider (33).

Surface Plasmon Resonance. Binding experiments using surface plasmon resonance were carried out on a ProteON XPR36 instrument (Bio-Rad). For this experiment, we used GLC sensor chips (Bio-Rad). To determine detection of Fab binding, FFL_001 was captured using the anti-his mAb (Immunology Consultants Laboratory, Clone 7B8). Mutated FFL_001 (R33C, N72Y, K82E) was used as a binding control. Fabs were injected as analytes in running buffer HBSEP+ (Teknova) with 1 mg/mL BSA at a flow rate of 50 μL/min. The surface was regenerated with 0.85% phosphoric acid (Bio-Rad), four injections, 15-s contact time each. We analyzed data using Proteon Manager software (Bio-Rad, v3.1.0.6). Binding responses were double referenced against interspot and reference channel. We fit the data with the Simple Binding Langmuir model.

HD Exchange Mass Spectrometry. Deuterium exchange was initiated by addition of 6.6 μL14N4 Fab (2.0 mg/mL) and 3.3 μL either scaffold (1.1 mg/mL) or water into 40 μL exchange buffer (100 mM NaCl, 20 mM Tris·HCl, pH 7.5) made in D_2O. For a nondeuterated control, the reaction was performed in the same buffer made in water. The reaction was allowed to proceed for 15, 30, or 60 min, and was quenched by addition of 50 μL quenching buffer (0.2% formic acid, 200 mM TCEP, 4 M urea, pH 2.45). The reaction was placed on ice, and 6.6 μL of porcine gastric pepsin (20 mg/mL) (Sigma-Aldrich) was added. Protease digestion was allowed to proceed for 5 min on ice, after which 100 μL was used for HPLC separation and mass spectrometric analysis. Each time point was performed in triplicate and the results averaged for analysis. The individual peptides were separated and analyzed for deuterium incorporation using a Rheodyne 7010 manual injector (Sigma-Aldrich) connected to a ThermoFinnigan Surveyor HPLC. Peptides were separated using Phenomenex 50 × 2.1 mm C18 reverse-phase column at 100 μL/min. Separation was performed using a 5–65% acetonitrile/H_2O gradient over 25 min, with 0.1% formic acid added to each buffer. The sample loop and column, as well as the chromatographic buffers, were completely submerged in an ice-water slurry to prevent excessive back exchange of deuterium atoms into the solvent. Mass spectra were recorded using a ThermoFinnigan LTQ XL ion trap mass spectrometer using positive ion electrospray ionization. The mass spectrometer was set to scan in the *m/z* range of 300–2,000, with the first 2 min of elution diverted to waste to eliminate early-eluting salts. For deuterium-exchange experiments, data were collected in MS1 mode. For peptide identification the same chromatography gradient was used, with the mass spectrometer run in data-dependent mode collecting seven scan events using collusion-induced dissociation fragmentation with a collision energy of 25 V. Peptide identification was done using PEAKS software (v7.0, Bioinformatics Solutions). Peptides were searched using a parent mass error tolerance of 0.5 Da and a fragment mass error tolerance of 0.5 Da, using nonspecific enzymatic cleavage and a charge state of 1–4. Posttranslation modifications of methionine oxidation and asparagine/glutamine deamidation were considered in peptide identification. Peptides were matched against a database consisting of 14N4 heavy and light chains, as well as porcine pepsin. Only peptides with a −10logP score of 35.3 or better were selected for deuterium exchange analysis, corresponding to a 0.05 false-discovery rate. Of all peptides identified, 15 with consistent signal and optimal coverage of all CDR loops were selected for deuterium-exchange analysis. The centroid mass of each peptide was calculated for each time point and compared with the nondeuterated control to calculate the extent of deuterium incorporation. The shift in mass compared with nondeuterated control was normalized by the theoretical upper limit of deuteration for each peptide to obtain the percent deuteration. Deuterium incorporation for an individual residue was calculated as a weighted average of all fragments containing the residue, weighted by the inverse of the peptide length. This normalization strategy has been used successfully to convert deuterium exchange values to a per-residue basis for structural visualization (34).

ACKNOWLEDGMENTS. We thank members of the J.E.C. laboratory, especially Nurgun Kose, Robin Bombardi, Rebecca Lampley, and Dr. Gopal Sapparapu for technical assistance; Dr. Jinhui Dong for helpful discussions regarding structure determination; and Dr. Joel Harp for technical assistance. A portion of the experiments described herein used the Vanderbilt robotic crystallization facility, which was supported by NIH Grant S10 RR026915. J.J.M. was supported by Grant T32 AI 07474, National Institute of Allergy and Infectious Diseases, NIH. The project was supported by the National Center for Advancing Translational Sciences Grant 2 UL1 TR000445-06. The content is solely the responsibility of the authors and does not necessarily represent the official views of the NIH.

1. Hall CB, et al. (2009) The burden of respiratory syncytial virus infection in young children. *N Engl J Med* 360(6):588–598.
2. Shefali-Patel D, et al. (2012) RSV hospitalisation and healthcare utilisation in moderately prematurely born infants. *Eur J Pediatr* 171(7):1055–1061.
3. Nair H, et al. (2010) Global burden of acute lower respiratory infections due to respiratory syncytial virus in young children: A systematic review and meta-analysis. *Lancet* 375(9725):1545–1555.
4. McLellan JS (2015) Neutralizing epitopes on the respiratory syncytial virus fusion glycoprotein. *Curr Opin Virol* 11:70–75.
5. IMpact RSV Study Group (1998) Palivizumab, a humanized respiratory syncytial virus monoclonal antibody, reduces hospitalization from respiratory syncytial virus infection in high-risk infants. *Pediatrics* 102(3):531–537.
6. Glenn GM, et al. (2016) A randomized, blinded, controlled, dose-ranging study of a respiratory syncytial virus recombinant fusion (F) nanoparticle vaccine in healthy women of childbearing age. *J Infect Dis* 213(3):411–422.
7. Smith G, et al. (2012) Respiratory syncytial virus fusion glycoprotein expressed in insect cells form protein nanoparticles that induce protective immunity in cotton rats. *PLoS One* 7(11):e50852.
8. Raghunandan R, et al. (2014) An insect cell derived respiratory syncytial virus (RSV) F nanoparticle vaccine induces antigenic site II antibodies and protects against RSV challenge in cotton rats by active and passive immunization. *Vaccine* 32(48):6485–6492.
9. Wu SJ, et al. (2007) Characterization of the epitope for anti-human respiratory syncytial virus F protein monoclonal antibody 101F using synthetic peptides and genetic approaches. *J Gen Virol* 88(Pt 10):2719–2723.
10. Correia BE, et al. (2014) Proof of principle for epitope-focused vaccine design. *Nature* 507(7491):201–206.
11. Crowe JE, et al. (1998) Monoclonal antibody-resistant mutants selected with a respiratory syncytial virus-neutralizing human antibody fab fragment (Fab 19) define a unique epitope on the fusion (F) glycoprotein. *Virology* 252(2):373–375.
12. Crowe JE, Jr, et al. (1998) Isolation of a second recombinant human respiratory syncytial virus monoclonal antibody fragment (Fab RSVF2-5) that exhibits therapeutic efficacy in vivo. *J Infect Dis* 177(4):1073–1076.
13. McLellan JS, et al. (2013) Structure of RSV fusion glycoprotein trimer bound to a prefusion-specific neutralizing antibody. *Science* 340(6136):1113–1117.
14. Wu H, et al. (2007) Development of motavizumab, an ultra-potent antibody for the prevention of respiratory syncytial virus infection in the upper and lower respiratory tract. *J Mol Biol* 368(3):652–665.
15. Beeler JA, van Wyke Coelingh K (1989) Neutralization epitopes of the F glycoprotein of respiratory syncytial virus: effect of mutation upon fusion function. *J Virol* 63(7): 2941–2950.
16. Smith SA, Crowe JE, Jr (2015) Use of human hybridoma technology to isolate human monoclonal antibodies. *Microbiol Spectr* 3(1):AID-0027–AID-2014.
17. McLellan JS, et al. (2013) Structure-based design of a fusion glycoprotein vaccine for respiratory syncytial virus. *Science* 342(6158):592–598.
18. Krarup A, et al. (2015) A highly stable prefusion RSV F vaccine derived from structural analysis of the fusion mechanism. *Nat Commun* 6:8143.
19. Anderson LJ, et al. (1985) Antigenic characterization of respiratory syncytial virus strains with monoclonal antibodies. *J Infect Dis* 151(4):626–633.
20. Zhao X, Chen FP, Sullender WM (2004) Respiratory syncytial virus escape mutant derived in vitro resists palivizumab prophylaxis in cotton rats. *Virology* 318(2): 608–612.
21. Zhao X, Sullender WM (2005) In vivo selection of respiratory syncytial viruses resistant to palivizumab. *J Virol* 79(7):3962–3968.
22. Zhao X, Chen F-P, Megaw AG, Sullender WM (2004) Variable resistance to palivizumab in cotton rats by respiratory syncytial virus mutants. *J Infect Dis* 190(11): 1941–1946.
23. Gilman MSA, et al. (2015) Characterization of a prefusion-specific antibody that recognizes a quaternary, cleavage-dependent epitope on the RSV fusion glycoprotein. *PLoS Pathog* 11(7):e1005035.
24. Luo X, et al. (2015) An epitope-specific respiratory syncytial virus vaccine based on an antibody scaffold. *Angew Chem Int Ed Engl* 54(48):14531–14534.
25. Wen X, et al. (2016) A chimeric pneumovirus fusion protein carrying neutralizing epitopes of both MPV and RSV. *PLoS One* 11(5):e0155917.
26. Yu X, McGraw PA, House FS, Crowe JE, Jr (2008) An optimized electrofusion-based protocol for generating virus-specific human monoclonal antibodies. *J Immunol Methods* 336(2):142–151.
27. Davidson E, Doranz BJ (2014) A high-throughput shotgun mutagenesis approach to mapping B-cell antibody epitopes. *Immunology* 143(1):13–20.
28. Sheldrick GM (2008) A short history of SHELX. *Acta Crystallogr A* 64(Pt 1):112–122.
29. Adams PD, et al. (2010) PHENIX: A comprehensive Python-based system for macromolecular structure solution. *Acta Crystallogr D Biol Crystallogr* 66(Pt 2):213–221.
30. Emsley P, Cowtan K (2004) Coot: Model-building tools for molecular graphics. *Acta Crystallogr D Biol Crystallogr* 60(Pt 12 Pt 1):2126–2132.
31. Kabsch W (2010) XDS. *Acta Crystallogr D Biol Crystallogr* 66(Pt 2):125–132.
32. Tang G, et al. (2007) EMAN2: An extensible image processing suite for electron microscopy. *J Struct Biol* 157(1):38–46.
33. Shaikh TR, et al. (2008) SPIDER image processing for single-particle reconstruction of biological macromolecules from electron micrographs. *Nat Protoc* 3(12):1941–1974.
34. Sevy AM, et al. (2013) Epitope mapping of inhibitory antibodies targeting the C2 domain of coagulation factor VIII by hydrogen-deuterium exchange mass spectrometry. *J Thromb Haemost* 11(12):2128–2136.